Engineered Migrasomes: A Robust, Thermally Stable Vaccination Platform

Dongju Wang[1,7], Haifang Wang[2,3,7], Wei Wan[2], Zihui Zhu[4], Takami Sho[1], Yi Zheng[1], Xing Zhang[5], Longyu Dou[6], Qiang Ding[4], Li Yu[1*] & Zhihua Liu[2*]

[1]The State Key Laboratory of Membrane Biology; Tsinghua-Peking Joint Center for Life Sciences; Beijing Frontier Research Center for Biological Structure; School of Life Sciences, Tsinghua University, Beijing 100084, China

[2]Institute for Immunology and School of Medicine, Tsinghua University, Beijing 100084, China

[3]Clinical Stem Cell Research Center, Peking University Third Hospital, Beijing, 100191, China.

[4]School of Medicine, Tsinghua University, Beijing 100084, China

[5]Ministry of Education Key Laboratory of Protein Sciences; Tsinghua-Peking Joint Center for Life Sciences; Beijing Advanced Innovation Center for Structural Biology; Beijing Frontier Research Center for Biological Structures; School of Life Science, Tsinghua University, Beijing, 100084, China

[6]Migrasome Therapeutics, Beijing, 102206, China

[7]These authors contributed equally

* Correspondence: Zhihua Liu, zhihualiu@mail.tsinghua.edu.cn;

Li Yu, liyulab@tsinghua.edu.cn

Abstract

The burgeoning abilities of pathogens and tumor cells to evade immune responses underscore the urgent need for innovative vaccination platforms based on a variety of biological mechanisms. The current logistical challenges associated with cold-chain (i.e. low-temperature) transportation particularly impacts access to vaccines in the global south. We recently discovered organelles called migrasomes, and herein we investigate the potential of migrasomes as an alternative vaccination platform. Their inherent stability and their enrichment with immune-modulating molecules make migrasomes promising candidates, but their low yield presents a hurdle. We address this problem through our engineered migrasome-like vesicles (eMigrasomes), which emulate the biophysical attributes of natural migrasomes with substantially improved yield. We show that eMigrasomes loaded with a model antigen elicit potent antibody responses and maintain stability at room temperature. We demonstrate that eMigrasomes bearing the SARS-CoV-2 Spike protein induce robust humoral protection against the virus. Our study demonstrates the potential of eMigrasome-based vaccines as a unique, robust, and accessible alternative to traditional methods.

Introduction

To face the imminent challenges of emerging infectious diseases, and to realize the not-yet-fulfilled promise of cancer vaccines, new types of vaccination platforms based on different basic biological principles are urgently needed. The huge success of mRNA vaccines in the fight against the Covid-19 pandemic further supports the importance of developing vaccine platforms based on different underlying biological mechanisms [1-4]. However, the application of mRNA-based vaccines, or other forms of traditional vaccine, has been hampered by the requirement for complicated cold-chain transportation, in which the materials are constantly maintained at low temperature [5, 6]. For most parts of the world, especially the global south, it is vitally important to develop vaccines which do not require cold-chain transportation.

Migrasomes are recently discovered organelles of migrating cells [7]. During migrasome formation, long membrane tethers named retraction fibers are pulled out at the trailing edge of migrating cells by the force generated by the movement of the cells. Migrasomes are formed on retraction fibers by a complicated process involving multiple components [8-10]. In the final expansion step, the growth of migrasomes is driven by assembly of nanometer-scaled tetraspanin-enriched microdomains (TEMs) into micrometer-scaled tetraspanin-enriched macrodomains (TEMAs) [9, 11]. Thus, migrasomes are highly enriched with components of TEMs — such as tetraspanins, integrins, and cholesterol — and formation of migrasomes is dependent on the presence of these molecules. For example, overexpression of Tspan4 can promote migrasome formation [9], while removing cholesterol can block migrasome formation. Theoretical

62 modelling, *in vitro* reconstitution of migrasome formation, and membrane stiffness
63 measurement by atomic force microscopy have revealed mechanistic insights into
64 migrasome formation. These approaches showed that tetraspanin- and cholesterol-
65 enriched macrodomains have highly elevated membrane stiffness, which is the key
66 factor to drive the bulging of retraction fibers into migrasomes; as a result, migrasomes
67 are highly rigid [9]. More recently, it was shown that assembly of TEMs can repair
68 damaged membranes by restricting the spread of membrane rupture. In liposomes
69 containing Tspan4 and cholesterol, detergent-induced membrane damage can be
70 rapidly repaired, and Tspan4-embedded liposomes are highly resistant to damage [12].
71 One defining feature of tetraspanin-enriched microdomains is the enrichment of
72 immune-modulating molecules such as members of the immunoglobulin superfamily
73 (IgSF) [13-15]. This group of molecules contains many key signaling molecular complexes
74 which regulate the immune response, including antigen receptors, antigen-presenting
75 molecules, co-receptors, antigen receptor accessory molecules, and co-stimulatory or
76 inhibitory molecules [16]. Since migrasomes are largely composed of TEMs, members of
77 the IgSF are also enriched in migrasomes. This property, in addition to the high stability
78 of migrasomes, prompted us to explore the possibility of developing a migrasome-
79 based vaccine.
80 One key obstacle to developing a migrasome-based delivery system and
81 migrasome-based vaccines is the very low yield of migrasomes. To generate
82 migrasomes, cells must be grown at very low density to allow them to migrate, and a
83 migrating cell can only generate a relatively low number of migrasomes in a process

84 that takes hours to finish [7]. In this study, by using the biophysical insights we gained
85 from investigating migrasome formation, we successfully overcome this key obstacle.
86 We developed a method which mimics the key biophysical features of migrasome
87 formation while vastly improving the yield of migrasome-like vesicles. We named
88 these vesicles as engineered migrasomes (eMigrasomes). Using eMigrasomes loaded
89 with the model antigen ovalbumin (OVA), we successfully demonstrate that
90 eMigrasomes are a highly effective, room temperature-stable vaccine platform which
91 generate a strong immunoglobulin G (IgG) response. Finally, we demonstrate that
92 eMigrasomes loaded with SARS-CoV-2 Spike protein (S protein) can generate a strong
93 protective humoral response against SARS-CoV-2. In summary, our study
94 demonstrates that the eMigrasome-based vaccine platform is stable at room temperature,
95 highly effective, and uses an unconventional immunological mechanism, which could
96 be useful in certain scenarios where conventional vaccine platforms are less successful.
97

98 **Results**

99 By serendipity, we found that hypotonic shock induces rapid formation of
100 migrasome-like structures on retraction fibers in Tspan4-GFP-expressing cells (Fig 1a).
101 Similar phenomena had also been observed in recent studies[17, 18] . 10 seconds after
102 hypotonic shock, the Tspan4 signal started to become enriched on retraction fibers.
103 These Tspan4-enriched domains then grew into migrasome-like structures. After
104 reaching its peak intensity, the Tspan4-GFP signal started to diffuse away from the
105 migrasome-like structure, which was accompanied by shrinkage of the migrasome-like

106 structure. 440 seconds after hypotonic shock, most of the hypotonic shock-induced
107 migrasome-like structures disappeared (Fig 1a, Supplementary Video 1). We found that
108 the size of the migrasome-like structures negatively correlated with osmolarity: the
109 lower the osmolarity, the larger the migrasome-like structures (Fig 1b, 1c). To study
110 the role of osmolarity in the formation of migrasome-like structures, we set up an
111 imaging protocol which allowed us to carry out live-cell imaging while lowering the
112 osmolarity in a step-wise manner (Fig 1d). We found that step-wise application of the
113 hypotonic shock significantly increased the duration time of the migrasome-like
114 structures. In cells undergoing 5 steps of hypotonic shock, 50% of the migrasome-like
115 structures were still stable 6 minutes after the final step of hypotonic shock; in contrast,
116 in cells undergoing one step of hypotonic shock, 50% of the migrasome-like structures
117 shrunk back or fused with their neighbors within 1.5 minutes. (Fig 1e, 1f,
118 Supplementary Video 2, 3).

119 We realized that the amount of migrasome-like structures generated by hypotonic
120 shock depends on the number of retraction fibers. We also realized that the majority of
121 the plasma membrane can be the source of membrane for migrasome-like structures.
122 We reasoned that if we shrink the cells by disrupting the cytoskeleton, the shrinkage
123 will cause the retraction of the cell edge toward the center. At the same time, the cells
124 will be adhering to the bottom of the culture plate at various points by focal adhesion.
125 These adhesion sites will keep the plasma membrane in place, thus serving as anchor
126 points for generation of membrane tethers. If this scenario is true, contraction of the
127 cell will generate large numbers of membrane tubes in a way similar to retraction fiber

128 formation during migration. To test this hypothesis, we treated cells with different doses
129 of latrunculin A (LatA), a reagent widely used for disruption of microfilaments, before
130 applying the step-wise hypotonic shock. As expected, we found that treating cells with
131 LatA caused shrinking of the cells. We also observed the massive formation of
132 membrane tethers in the area which was occupied by the cell before shrinkage.
133 Importantly, we observed significantly enhanced formation of migrasome-like
134 structures from these newly formed membrane tethers in a LatA dose-dependent
135 manner (Fig 1g, 1h).

136 It is well established that cells can counter a change of osmolarity with regulated
137 volume change [19]. To test whether regulated volume change can affect the formation of
138 migrasome-like structures, we knocked down SWELL1, a key component of the
139 volume-regulated anion channel which maintains a constant cell volume in response to
140 osmotic changes [20, 21]. We found that knockdown of SWELL1 significantly enhanced
141 the formation of migrasome-like structures. This result suggests that formation of
142 migrasome-like structures can be enhanced by reducing the capacity of cells to regulate
143 their volume during osmolarity change (Fig 1i - 1k).

144 Under normal physiological conditions, the extracellular space typically contains a
145 substantial amount of sodium. Throughout all the aforementioned experiments, the
146 buffer employed predominantly consisted of sodium as the prevailing cation. Cations
147 are known for their role in regulation of cell volume. Next, we tested the effect of
148 different cations on the formation of migrasome-like structures. We reasoned that if
149 different cations have different abilities to regulate cell volume during osmolarity

150 change, we may be able to find an easy way to attenuate the regulated cell volume
151 change, thus promoting the formation of migrasome-like structures. To do that, we first
152 replaced the medium with isotonic buffers containing different cations, then we added
153 water step-wise to reduce the osmolarity. We found that indeed different cations have
154 different abilities to promote the generation of migrasome-like structures. Substitution
155 of sodium with equal molar potassium, cesium or choline significantly enhanced the
156 generation of migrasome-like structures (Fig 1l, 1m).

157 Tspan4 is the key protein that promotes migrasomes formation, and all the
158 experiments described above were carried out in Tspan4-GFP-expressing cells. To test
159 whether Tspan4 can promote the formation of migrasome-like structures, we treated
160 mCherry- or Tspan4-mCherry-expressing cells with step-wise hypotonic shock, and
161 then observed the formation of migrasome-like structures by WGA staining, which
162 labels migrasomes effectively [22]. We found that indeed Tspan4-mCherry significantly
163 enhanced the formation of migrasome-like structure (Fig 2a, 2b). Similar results held
164 for Tspan1 and CD82, which are also migrasome-promoting tetraspanins (Fig 2c, 2d,
165 S1a, S1b). Previously, we reported that cholesterol is essential for migrasome formation.
166 We treated cells with methyl-beta-cyclodextrin (MβCD), which selectively extracts
167 cholesterol from the plasma membrane. We found that addition of MβCD rapidly
168 destroyed the readily formed migrasome-like structures (Fig 2e, 2f). This suggests that,
169 similar to migrasomes, the structural integrity of migrasome-like structures depends on
170 cholesterol. Recently, we reported that formation of migrasomes is dependent on SMS2.
171 We found that treating cells with SMS2-IN-1, a selective inhibitor of SMS2,

172 significantly inhibits the formation of migrasome-like structures (Fig 2g, 2h). Finally,
173 we tested whether the formation of migrasome-like structures can occur in cells other
174 than NRK cells. Indeed, all the cells we tested were able to support the formation of
175 migrasome-like structures (Fig 1n).

176 Because of the mechanistic similarity between migrasomes and migrasome-like
177 structures (Fig 2i), and because of the artificial nature of the procedure to generate these
178 structures, we named these migrasome-like structures as engineered migrasomes
179 (eMigrasomes).

180 Based on these results, we designed a protocol to generate and isolate eMigrasomes
181 (eMigs) (Fig 3a). In this protocol, cells cultured in flasks were pretreated with high-
182 potassium DPBS (K-DPBS) containing LatA and then the osmolarity was reduced by
183 adding water in a step-wise manner. The flask then was subjected to moderate rotation
184 to separate poorly-adhering cell bodies and tightly-adhering eMigs. The supernatant
185 containing the majority of cell bodies was discarded and the eMigs attached to the
186 bottom were harvested by pipetting. No trypsinization was applied to ensure optimal
187 protection of the integrity of eMigs. To remove remaining cell bodies, crude eMigs
188 were subjected to differential centrifugation followed by a gravity-dependent filtration
189 through a 6-μm filter. eMigs in the flowthrough were concentrated by high-speed
190 centrifugation. This protocol generated eMigs in a high yield. By microscopic
191 examination, every individual cell robustly generates eMigs (Supplementary Video 4).
192 By confocal microscopy analysis, the isolated eMigrasomes are round vesicles with
193 different sizes (Fig 3b). To measure the size of eMigrasomes, we carried out a confocal-

194 based analysis using Hough circle transformation (Fig 3b). We found that eMigrasomes
195 have a size range from 1.4 μm - 6.6 μm, with a median size of 1.6 μm (Fig 3c). Since
196 negative staining might distort the shape of membrane vesicles (Fig 3d), we carried out
197 cryo-EM analysis of eMigrasomes. Under cryo-EM, eMigrasomes appeared as intact
198 round vesicles (Fig 3e). Notably, the eMigs were not contaminated with significant
199 amounts of intracellular membranes, as western blotting of purified eMigs showed very
200 little contamination from other organelles (Fig 3f).

201 Previously we reported that migrasomes can become leaky before rupture. We
202 wondered whether eMigrasomes can also become leaky. To test this, we added
203 eMigrasomes into isolation buffer loaded with Cy5 and 40 kDa dextran-TMR. At room
204 temperature, eMigrasomes rapidly become leaky to Cy5, a fluorescent dye that does
205 not pass intact membranes (Fig 3g). During the 48 hours after preparation,
206 eMigrasomes gradually become leaky to 40 kDa dextran-TMR, which mimics the size
207 of a normal protein (Fig 3g, 3h).

208 Next, we tested the stability of eMigrasomes at room temperature. Surprisingly,
209 eMigrasomes are highly stable. Even after 14 days at room temperature, the
210 morphology of eMigrasomes did not change significantly, and the number of
211 eMigrasomes was only slightly reduced (Fig 3i, 3j). However, if we treated isolated
212 eMigrasomes with MβCD, most of them deformed and ruptured within 30 min (Fig 3k).
213 This suggests a crucial contribution of cholesterol to the stability of isolated
214 eMigrasomes.

215 The stable nature of eMigs prompted us to explore the possibility of using eMigs
216 as carriers for delivery of proteins (Fig 4a). We found that membrane proteins (e.g. the
217 cell surface receptor PD1) can be easily loaded onto eMigrasomes by simply
218 overexpressing these proteins in cells (Fig 4b). To load cytosolic proteins, we fused
219 them with the transmembrane domain followed by the polybasic tail of syntaxin 2
220 (STX2). This allowed us to successfully load the cytosolic protein ovalbumin (OVA)
221 onto the plasma membrane and thus onto eMigrasomes, referred as mOVA for
222 membrane-tethered OVA (Fig 4c).

223 **An eMigrasome-based vaccine**

224 Next, we explored the potential of eMigrasomes as an antigen carrier for vaccines.
225 First, we employed OVA, a well-established model antigen, to evaluate eMigrasomes
226 as a platform for antigen delivery. We used imaging and immunoblotting to confirm
227 the presence of the mOVA-mCherry protein (Fig 4d, 4e). It is worth noting that the
228 mOVA antigen was highly enriched in isolated eMigrasomes compared to the host cells
229 (Fig 4e). We immunized mice with OVA-loaded eMigrasomes (eM-OVA) via different
230 routes and found that intravenous injection resulted in the highest IgG antibody titer
231 (Fig 4f). eM-OVA induced the antigen-specific IgG response in a dose-dependent
232 manner (Fig 4g). The IgG response induced by eM-OVA at 20 μg/mouse was
233 comparable to traditional Alum/OVA at 50 μg/mouse (Fig 4h). Together, these data
234 suggest that eM-OVA elicits a strong IgG response compared to traditional alum-based
235 immunization.

236 Next, we assessed the stability of the immunogenicity of eM-OVA over a period
237 of 14 days at room temperature. For this purpose, we placed the purified OVA-loaded
238 eMigrasomes in a test tube at room temperature without adding any reagents to inhibit
239 protein degradation. After 14 days of room temperature storage, the amount of intact
240 OVA was roughly the same as in freshly purified eM-OVA, and the IgG response
241 induced by eM-OVA remained unchanged during this period (Fig 4i - 4k).

242 **An eMigrasome-based vaccine induces a strong humoral protective response**
243 **against SARS-CoV-2**

244 We next explored eMigs as a platform to carry the SARS-CoV-2 Spike protein (S
245 protein). To prevent the S protein from being broken down by proteases, we mutated
246 the furin site of the S protein. MCA-205 cells were used to express the S protein with
247 an mCherry tag. After isolating the eMigs, we used imaging to confirm the presence of
248 the Spike protein (Fig 5a). Immunization of WT C57BL/6J mice with the Spike-loaded
249 eMigs (eM-S) resulted in a strong antibody response against the S protein, which was
250 further improved by a second shot (Fig 5b, 5d). To assess the neutralizing capacity of
251 the antisera provoked by eM-S, we utilized a replication-competent, infectious VSV
252 chimera incorporated with the SARS-CoV-2 spike protein for a neutralization test (Fig
253 5c), similar to the previously reported system[23, 24]. This genetically altered VSV
254 chimera virus features the SARS-CoV-2 spike protein, substituting its native surface
255 glycoprotein (G), making the VSV chimera reliant on the SARS-CoV-2 spike protein
256 for cellular entry. The Venus-based fluorescence reporter system offers high sensitivity.
257 The neutralizing power of antisera against the SARS-CoV-2 spike protein was assessed

258 by calculating the percentage of Venus-positive infected cells when treated with serum
259 versus mock controls. The antisera, stimulated by an initial immunization with eM-S,
260 neutralized the recombinant VSV-Venus-SARS-CoV2 up to a dilution titer of
261 approximately 300 to achieve 50% neutralization (NT_{50}). A secondary booster
262 immunization further enhanced the neutralization capability with an NT_{50} up to 4000
263 (Fig 5e, 5f). Together, these results indicate that antigen-carrying eMigs can induce a
264 strong humoral protective response against SARS-CoV-2.
265
266 **Discussion**
267 In this manuscript, we describe a method to rapidly generate eMigrasomes from
268 cultured mammalian cells. We developed a simple method to load membrane or
269 cytosolic proteins onto eMigrasome. Using OVA as a model antigen, we demonstrate
270 that eMigrasomes are a highly effective, temperature-stable vaccine platform which can
271 elicit antibody response with a very small amount of antigen. Finally, we show that
272 eMigrasomes can be used to generate effective vaccines against SARS-CoV-2.
273 Collectively, our study provides the proof of concept for developing eMigrasome-based
274 vaccines.
275 In this study, we demonstrate the efficiency of eMigrasome-based vaccines using
276 a model antigen or an antigen from a coronavirus. The benefit of using a model antigen
277 is that there are readily available experimental systems. The benefit of using a well-
278 characterized virus antigen is that it allows us to reliably test the efficacy of our vaccine
279 platform in a realistic setting. We are aware that due to the experimental nature of this

280 work, it is unlikely that the eMigrasome platform will be used to generate mainstream
281 preventive vaccines in the foreseeable future. However, there is a very real possibility
282 of developing eMigrasomes into therapeutic vaccines against cancer or other diseases
283 with unmet medical needs, or into preventive vaccines against pathogens for which the
284 current vaccine platforms do not work. Our investigation regarding the biophysical and
285 cellular mechanisms of eMigrasome formation makes it possible for further optimizing
286 eMigrasome generation in a rational manner.

287 In this study, we demonstrate that eMigrasomes can be an effective vaccine
288 platform. In addition, we speculate that eMigrasomes may also emerge as a versatile
289 delivery system for a range of applications. The high rigidity and self-repair capacity
290 of migrasomes, which is caused by enrichment of tetraspanins and cholesterol, makes
291 migrasomes highly stable, and thus suitable as delivery carriers in various *in vivo*
292 settings. More importantly, the physiological roles of migrasomes indicate that they
293 have naturally evolved as carriers for delivering materials and information *in vivo*. Our
294 previous work showed that during embryonic development, migrasomes which are
295 highly enriched with signaling molecules, such as chemokines, growth factors and
296 morphogens, are deposited at various spatially defined locations, where they act as
297 sustained-release capsules to liberate the signaling molecules. In this way, migrasomes
298 affect multiple aspects of embryonic development including organ morphogenesis and
299 angiogenesis [25, 26]. Additionally, in cultured fibroblast cells, migrasomes are enriched
300 with a selected set of full-length, translationally competent mRNAs. When these
301 mRNA-enriched migrasomes are taken up by neighboring cells, the mRNA can escape

302 the endo-lysosome system of recipient cells and be translated into protein, thus
303 modifying the behaviors of the recipient cells [27]. Finally, in cells experiencing mild
304 mitochondrial damage, the damaged mitochondria can be selectively transported into
305 migrasomes and then evicted from the cell in a process named as mitocytosis [28]. In
306 summary, multiple types of cargos, including materials and information, can be
307 enriched in migrasomes under different settings, and migrasomes can be deposited at
308 spatially defined locations in diverse biological settings to affect a broad range of
309 biological processes, including cell-cell communication. Since eMigrasomes capture
310 certain key features of migrasomes, it is our speculation that we may able to develop
311 eMigrasomes into a delivery system for diverse cargo types including nucleic acids,
312 proteins, small molecules and even organelles.
313

Figures and Figure Legends

Fig. 1

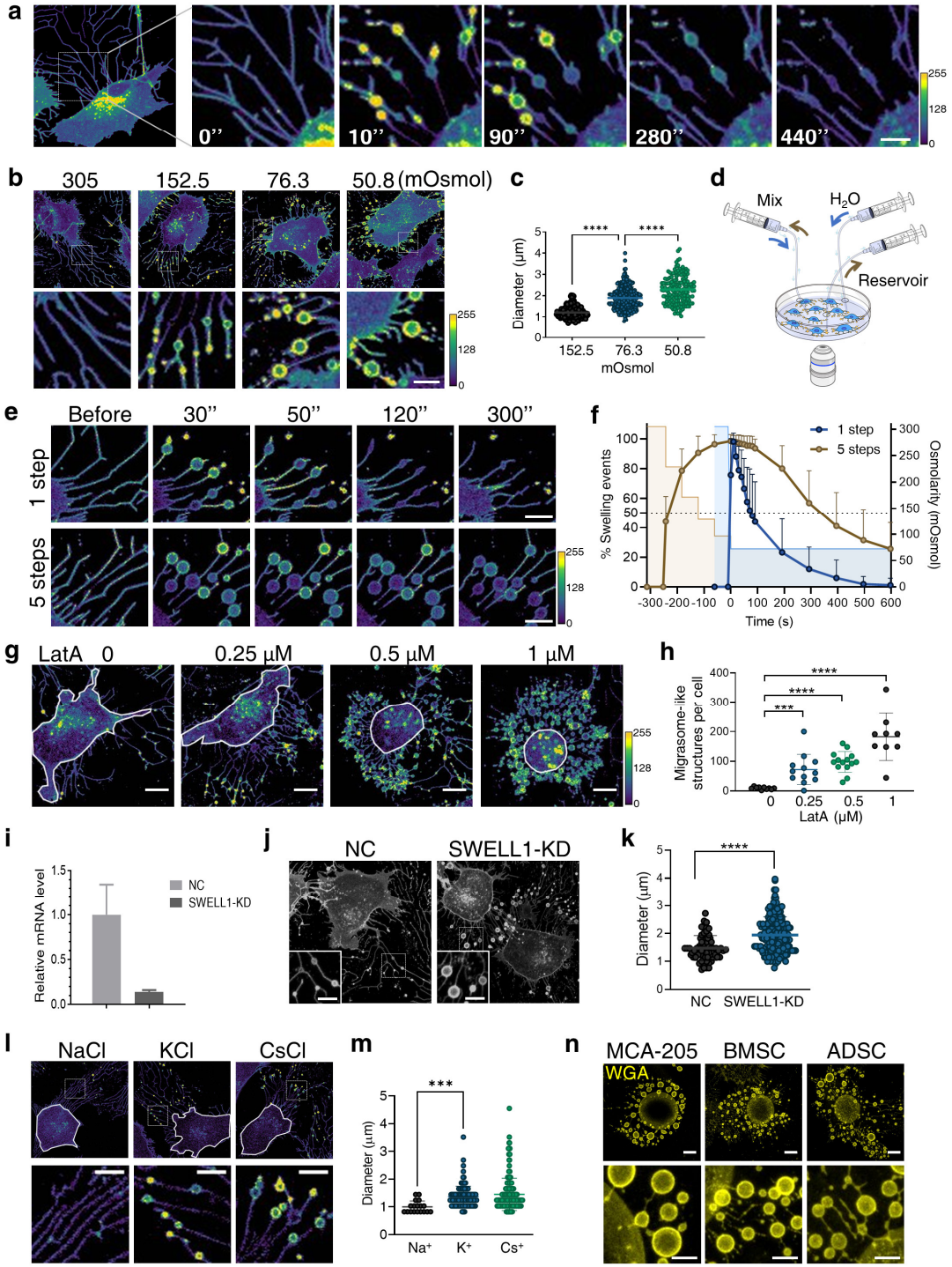

Figure 1 | Hypotonic stimulation induced migrasome-like structures

(a-m) The biogenesis of migrasome-like structures in NRK cells stably expressing

318 Tspan4-GFP. In these images, the fluorescence intensity of Tspan4-GFP is shown in a
319 color map scale from purple (low) to yellow (high).
320 (a) Image series of the biogenesis of migrasome-like structures. Cells were treated with
321 hypotonic Dulbecco's phosphate-buffered saline (DPBS) with an osmolarity of 76.3
322 mOsmol and imaged using a confocal microscope. Scale bar, 10 μm.
323 (b) Representative confocal images of cells treated with DPBS with various
324 osmolarities. 305 mOsmol represents an isotonic condition in which no migrasome-like
325 structures were observed. DPBS diluted to 152.5, 76.3 or 50.8 mOsmol was used to
326 achieve hypotonic stimulations of different magnitude. The size of migrasome-like
327 structures increased as the osmolarity was reduced. Scale bar, 5 μm.
328 (c) For each migrasome-like structure in (b), the whole lifetime, including the growth
329 and shrinkage, was recorded by time-lapse imaging. The largest diameter reached
330 during the lifetime was measured. The average diameter of migrasome-like structures
331 increased significantly as the osmolarity was reduced. For hypotonic stimulation at
332 152.5, 76.3 or 50.8 mOsmol, n = 194, 261, 165 migrasome-like structures, respectively.
333 (d) Illustration of the experimental setup for real-time imaging of the induction of
334 migrasome-like structures.
335 (e) Image series of cells treated with hypotonic DPBS in two different approaches. The
336 osmolarity of DPBS was reduced to 76.3 mOsmol by either one single step (upper panel)
337 or five steps with 1 min intervals (lower panel). For the step-wise reduction, the
338 osmolarity was lowered by 25% in each step. Imaging time-points were counted from

339 the final stimulation step. Migrasome-like structures induced by the stepwise protocol
340 showed significantly enhanced stability. Scale bar, 5 μm.
341 (f) Statistical analysis of growth curves of migrasome-like structures in (e). For single
342 step stimulation, n = 16 cells; for step-wise stimulation, n = 13 cells.
343 (g) Representative confocal images showing the effect of Latrunculin A (LatA)
344 treatment on the biogenesis of migrasome-like structures. Cells were pre-incubated
345 with 0, 0.25, 0.5 or 1 μM LatA for 10 mins and then treated with a five-step hypotonic
346 stimulation as described in (e). LatA enhanced the biogenesis of migrasome-like
347 structures in a dose-dependent manner. The white line indicates the boundary of the
348 cell body. Scale bar, 10 μm.
349 (h) Statistical analysis of the number of migrasome-like structures per cell in (g). n =
350 9-14 cells.
351 (i) Relative mRNA level of SWELL1 analyzed by qPCR. SWELL1 expression was
352 significantly reduced in SWELL1-knockdown (KD) cells compared to control cells.
353 (j) Representative confocal images of control or SWELL1-KD cells. Cells were treated
354 with a five-step hypotonic stimulation at 2 min intervals. The osmolarity was reduced
355 by 1/6 in each step. Migrasome-like structures are shown in the inserts. Scale bar, 5 μm.
356 (k) Statistical analysis of the diameter of migrasome-like structures in (j); n=75 for
357 control cells and 104 for SWELL1-KD cells.
358 (l) Representative confocal images showing the effect of extracellular cations on the
359 biogenesis of migrasome-like structures. Before stimulation, culture medium was
360 replaced by modified DPBS in which either Na^+, K^+ or Cs^+ was the only cation source.

361 Cells were then treated with a five-step hypotonic stimulation at 2 min intervals. The
362 osmolarity was reduced by 1/6 in each step. Scale bar, 5 μm.
363 (m) Statistical analysis of the diameter of migrasome-like structures in (l); n = 18 for
364 Na^+, 119 for K^+ and 203 for Cs^+.
365 (n) Multiple primary cell types and cell lines are capable of producing eMigrasomes.
366 Cells were stained with WGA-AF488 (Thermo, W11261) after hypotonic induction of
367 eMigrasome with our protocol. Z-stack image series were captured and sum-slices
368 projections were applied. Scale bar, 10 μm (upper panels) and 5 μm (lower panels).
369 For all statistical analyses in this figure, *P* values were calculated using a two-tailed
370 unpaired nonparametric test (Mann-Whitney test). *P* value<0.05 was considered
371 statistically significant. *** *P*<0.001. **** *P*<0.0001.
372

Fig. 2

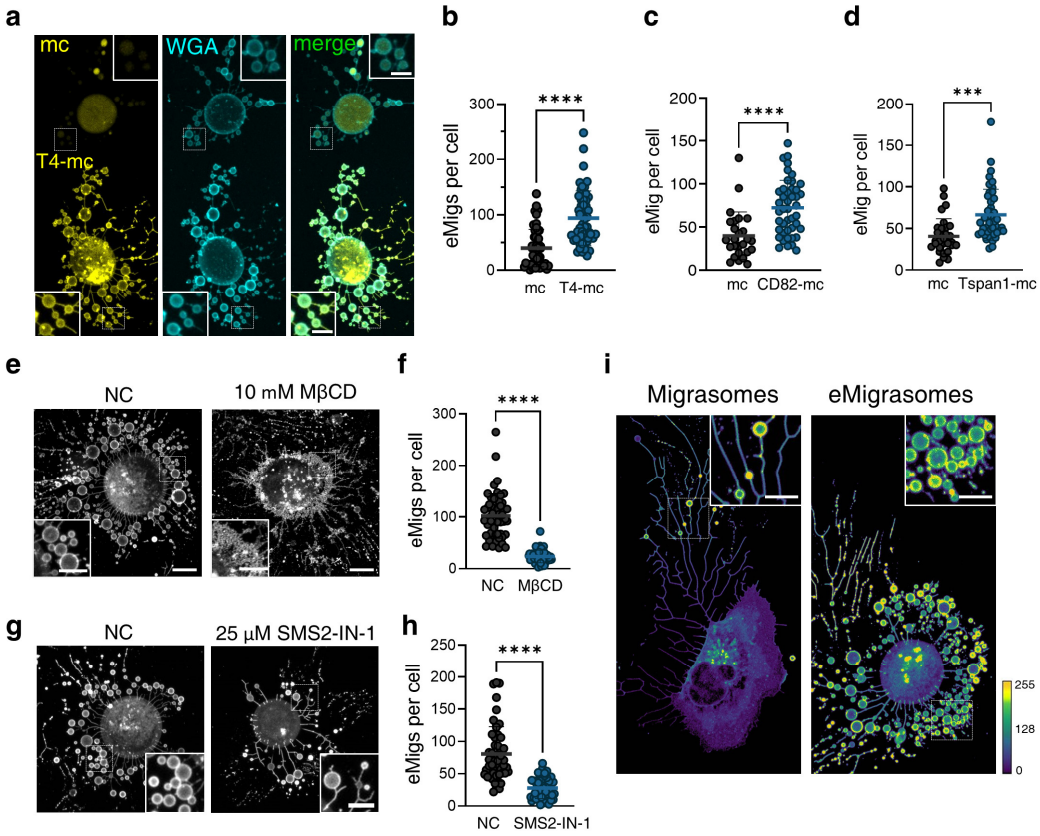

Figure 2 | Mechanistic and morphologic similarity between migrasomes and eMigrasomes

(a) Representative confocal images showing the effect of Tspan4-GFP in the biogenesis of migrasome-like structures. NRK cells were transiently transfected with mCherry vector or Tspan4-mCherry. The two populations of transfected cells were mixed in a 1:1.5 ratio in a test tube and then seeded in a confocal chamber. Cells were pre-incubated with 2 μM LatA for 10 mins and then treated with a three-step hypotonic stimulation with 2 min intervals. In each step, the osmolarity was reduced by 1/6 (16.7%). WGA-AF647 (Thermo, W32466) was then added to stain migrasome-like structures. Z-stack images were captured for further analysis. Scale bar, 5 μm.

384 (b) Statistical analysis of the number of migrasome-like structures per cell in NRK cells
385 transiently transfected with mCherry vector or Tspan4-mCherry in (a). n = 53, 53 cells
386 respectively.
387 (c) Statistical analysis of the number of migrasome-like structures per cell in NRK cells
388 transiently transfected with mCherry vector (n = 26 cells) or CD82-mCherry (n = 44
389 cells) in Fig S1a.
390 (d) Statistical analysis of the number of migrasome-like structures per cell in NRK cells
391 transiently transfected with mCherry vector (n = 31 cells) or Tspan1-mCherry (n = 44
392 cells) in Fig S1b.
393 (e) Representative confocal images showing the effect of cholesterol extraction on
394 migrasome-like structures. NRK cells stably expressing Tspan4-GFP were stimulated
395 to generate migrasome-like structures as described in (a). Cells were then incubated
396 with 10 mM MβCD or buffer supplied with an equal volume of control solvent (H_2O)
397 for 30 min before imaging. Z-stack images were captured for further analysis. Scale bar,
398 10 μm. Insert scale bar, 5 μm.
399 (f) Statistical analysis of the number of migrasome-like structures per cell in control
400 cells (n=56) or cells treated with 10 mM MβCD (n=58) in (e).
401 (g) Representative confocal images showing the effect of sphingomyelin depletion on
402 the biogenesis of eMigrasomes. NRK cells stably expressing Tspan4-GFP were
403 incubated with DMSO or 25 μM SMS2-IN-1 for 16 hrs. Cells were then treated and
404 imaged as described in (a). Scale bar, 5 μm

405 (h) Statistical analysis of the number of migrasome-like structures per cell in control
406 cells (n=51) or cells treated with 25 μM SMS2-IN-1 (n=46) in (g).
407 (i) Representative confocal images showing a cell generating natural migrasomes (left)
408 and eMigrasomes (right). Migrasomes and eMigrasomes are morphologically similar.
409 The fluorescence signal of Tspan4-GFP is highly enriched in both migrasomes and
410 eMigrasomes.

Fig. 3

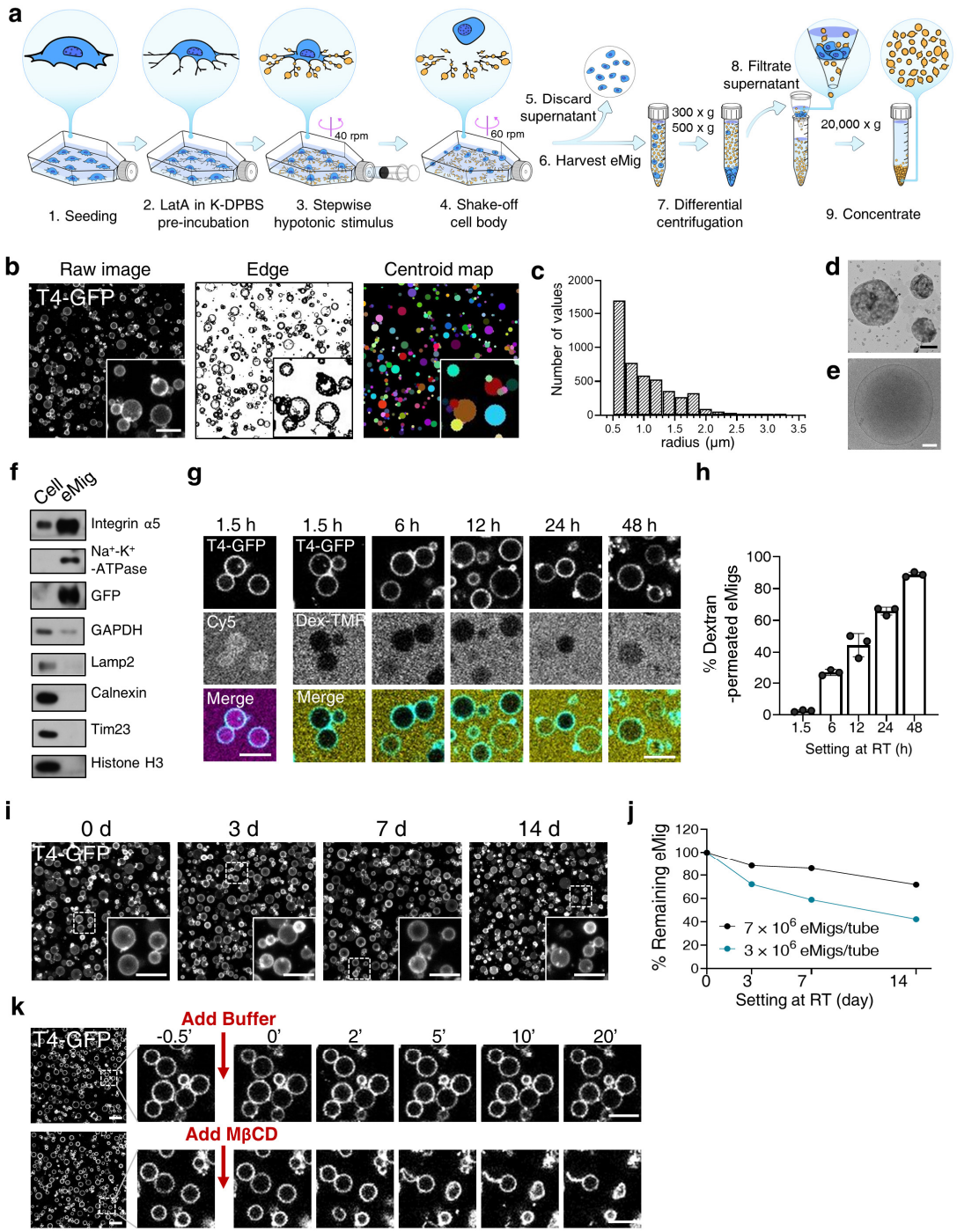

Figure 3 | Isolation and characterization of eMigrasome

NRK cells stably expressing Tspan4-GFP were used in all experiments in this figure if not otherwise specified.

415 (a) Schematic illustration showing the process of eMigrasome induction, isolation and
416 purification.
417 (b) Confocal image (left), threshold edge (middle) and centroid map (right) of purified
418 eMigrasomes. Image processing and analysis were performed using imageJ. The Hough
419 circle transform plugin was applied to recognize and transform thresholded edges into
420 binned objects representing individual eMigrasomes. Scale bar, 5 μm
421 (c) Statistical analysis of the radius of purified eMigrasomes. Measurement was
422 performed using the map generated by Hough circle transformation analysis. 4725
423 particles were analyzed and the data were binned to plot the distribution of
424 eMigrasomes radius.
425 (d) TEM micrograph of negatively stained purified eMigrasomes. Scale bar, 1 μm.
426 (e) Cryo-EM micrograph of purified eMigrasomes. Scale bar, 200 nm.
427 (f) Western blot showing the protein level of several markers in cell bodies and
428 eMigrasomes. An equal amount of protein was loaded in each lane.
429 (g) Representative time-lapse confocal images showing the high permeability of
430 eMigrasomes to Cy5 at 1.5 hrs post purification (left) and the gradual increase in the
431 permeability of eMigrasomes to 40 kDa dextran-TMR (right). Scale bars, 5 μm
432 (h) Statistical analysis of the percentage of eMigrasomes that were permeable to 40 kDa
433 dextran-TMR at the indicated timepoints. For each time point, eMigrasomes from three
434 different views were analyzed. From left to right, n = 336, 493, 812, 830 and 631.
435 (i) Representative confocal images of eMigrasomes after sitting at room temperature
436 for 0, 3, 7 or 14 days. Aliquots of eMigrasomes were stored in EP tubes as pellets at

437 room temperature for the indicated time, then resuspended and dropped into a confocal
438 chamber before imaging. Z-stack image series were captured and sum-slices
439 projections were applied. Scale bar, 5 μm.
440 (j) Number of eMigrasomes after storage at room temperature for 0, 3, 7 or 14 days.
441 Aliquots of eMigrasomes (7 x 10^6 eMigrasomes per tube in black, 3 x 10^6 eMigrasomes
442 per tube in green) were stored in EP tubes as pellets at room temperature for the
443 indicated time, then resuspended and stained with WGA561 before counting by FACS.
444 (k) Time-lapse image series showing purified eMigrasomes treated with 10 mM MβCD
445 or control buffer. A 10 μl drop of concentrated eMigrasomes was settled in a confocal
446 chamber, then sealed and maintained at 37°C during imaging. Buffer containing 10 mM
447 MβCD or control solvent was added to the drop using the equipment illustrated in Fig
448 1d. Scale bar, 5 μm
449

Fig. 4

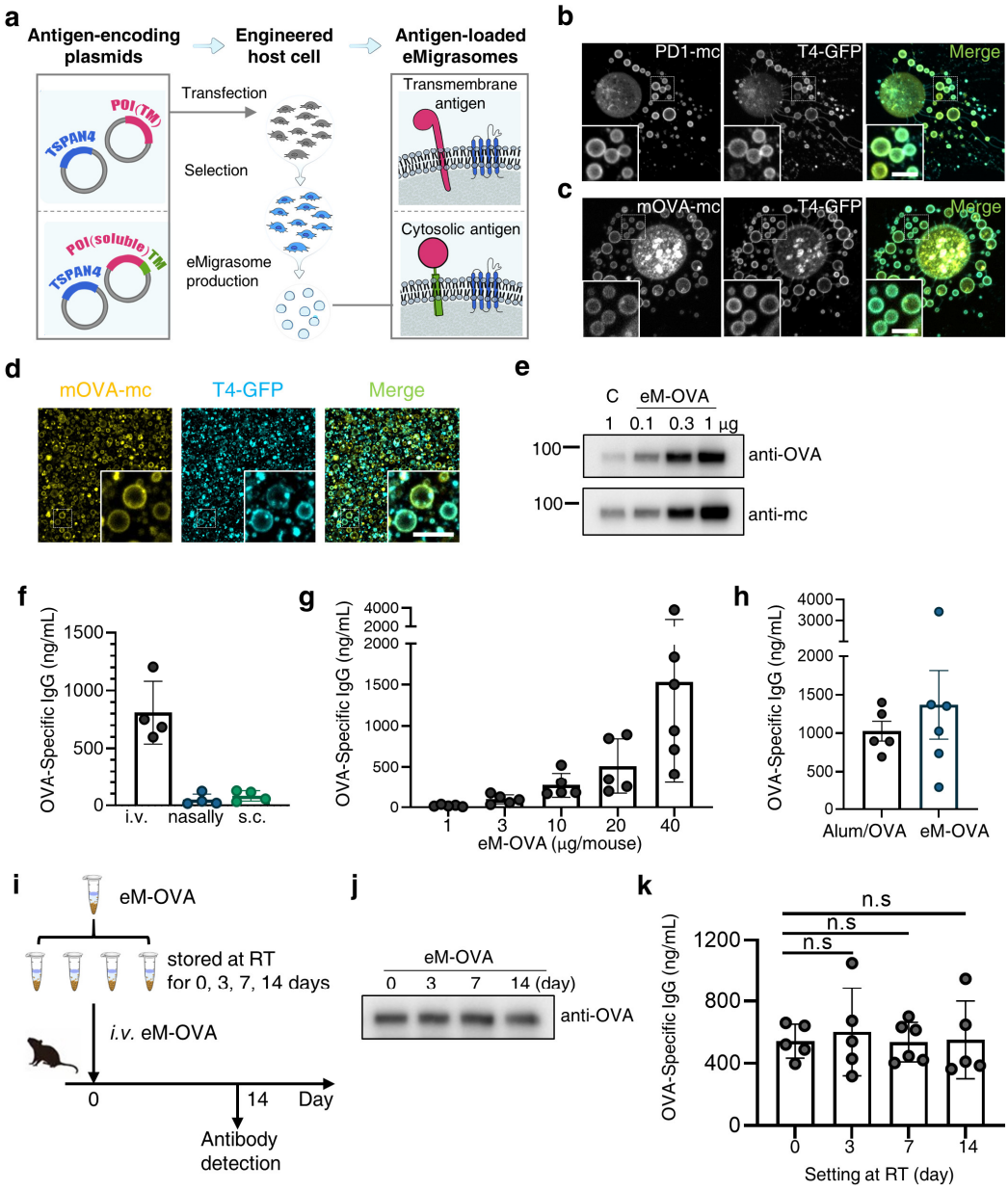

450

451 **Figure 4 | eMigrasomes as an antigen carrier for vaccination**

452 (a) Schematic illustration of strategies for loading proteins of interest (POI) onto
453 eMigrasomes. The protocol includes the construction of antigen-encoding plasmids, the
454 construction of engineered cell lines stably expressing the antigens and the production
455 of antigen-loaded eMigrasomes. Membrane proteins, which already carry a
456 transmembrane (TM) domain, are overexpressed in cells (top). Cytosolic proteins are

457 membrane tethered by tagging with the TM sequence and polybasic tail of STX2
458 (bottom). Cells are then treated with hypotonic buffer to enrich the POI on the surface
459 of eMigrasomes.
460 (b) Representative confocal image of a cell expressing PD1-mCherry and Tspan4-GFP.
461 The transmembrane protein PD1-mCherry was loaded onto eMigrasomes as shown in
462 the top part of (a). Scale bar, 5 μm
463 (c) Representative confocal image of a cell expressing membrane-tethered OVA-
464 mCherry (mOVA-mc) and Tspan4-GFP. To create an extracellular membrane- tethered
465 form of OVA (mOVA), the sequence of OVA was fused to the C-terminus of a
466 truncated form of mouse STX2, in which only the transmembrane region and a
467 polybasic tail remained. The mCherry tag was fused to the C-terminus of OVA to trace
468 the localization of this fusion protein. The soluble protein OVA was loaded onto the
469 membrane of eMigrasomes, as shown in the bottom part of (a). Scale bar, 5 μm.
470 (d) Representative confocal image of eMigrasomes isolated from MCA-205 cells stably
471 expressing Tspan4-GFP and mOVA-mCherry (eM-OVA). Scale bar, 5 μm.
472 (e) Western blot showing the amount of full-length mOVA-mCherry protein in host
473 cell and eM-OVA. Cell lysate (C) containing 1 μg total protein and purified eM-OVA
474 samples containing 0.1, 0.3 or 1 μg total protein were loaded. The protein-immobilized
475 PVDF membrane was firstly incubated with anti-OVA antibody and then stripped and
476 re-blotted with anti-mCherry antibody. The antigen mOVA-mCherry was highly
477 enriched in eMigrasomes compared to host cells.

478 MCA-205 cells stably expressing Tspan4-GFP and mOVA-mCherry were used for all
479 experiments in the rest of this figure if not otherwise specified.
480 (f) Amount of OVA-specific IgG in mouse serum on day 14 after intravenous (i.v),
481 nasal or subcutaneous (s.c) immunization with eM-OVA (20 μg/mouse). OVA-specific
482 IgG was quantified by ELISA.
483 (g) ELISA quantification of OVA-specific IgG in sera from wild-type (WT) mice on
484 day 14 after tail intravenous immunization with eM-OVA at the indicated dose.
485 (h) ELISA quantification of OVA-specific IgG in sera from WT mice on day 14 after
486 tail intravenous immunization with eM-OVA (20 μg/mouse) or intraperitoneal
487 immunization with Alum/OVA.
488 (i) Illustration of the experimental setup for assaying the stability of eM-OVA.
489 (j) Immunoblotting analysis of the amount of OVA protein in samples of eM-OVA
490 which were left at room temperature for 0, 3, 7 or 14 days. 2 μg protein was loaded in
491 each lane.
492 (k) ELISA quantification of OVA-specific IgG in sera from WT mice on day 14 after
493 tail intravenous immunization with eM-OVA stored at room temperature for 0 days
494 (D0), 3 days (D3), 7 days (D7) or 14 days (D14). 20 μg eM-OVA was injected per
495 mouse.

Fig. 5

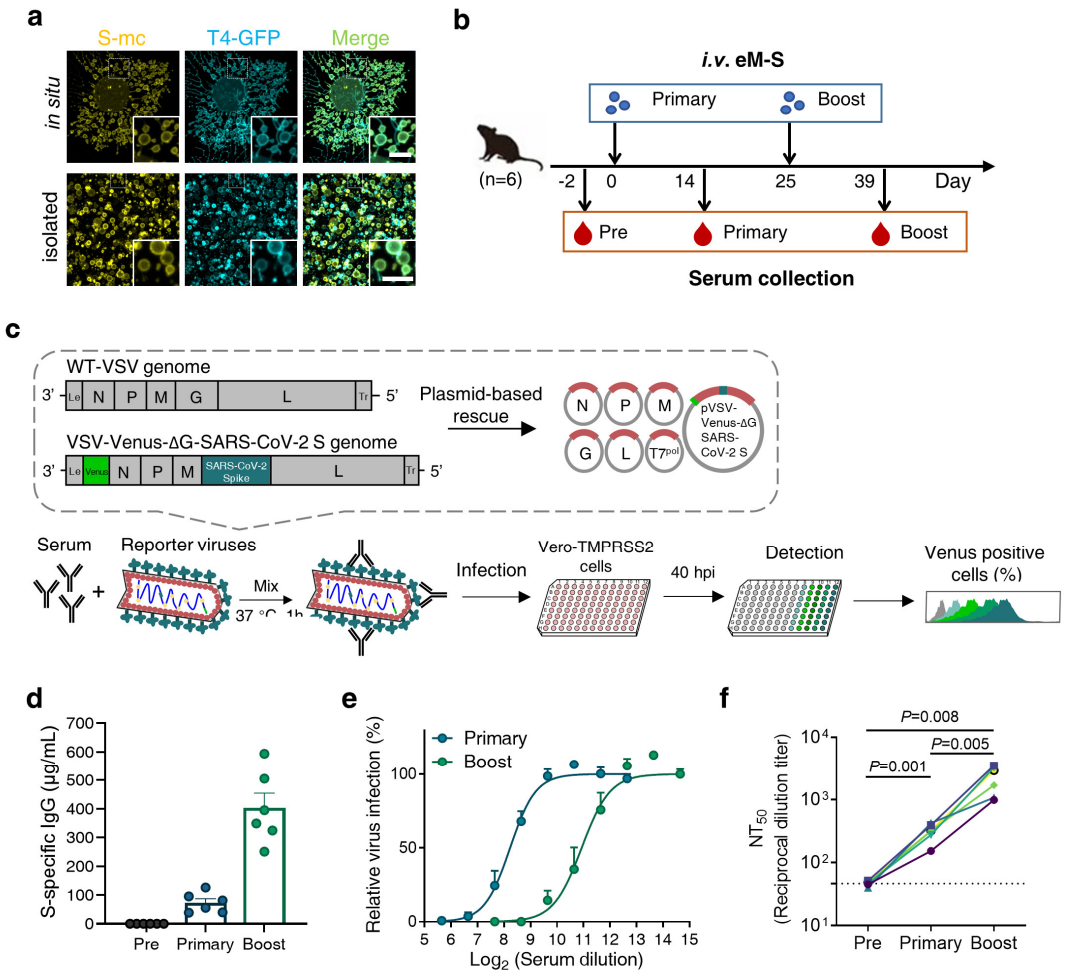

Figure 5 | An eMigrasome-based vaccine induces a strong humoral protective response against SARS-CoV-2

(a) Representative confocal images showing the presence of Spike-mCherry (S-mc) in engineered cells and isolated eMigrasomes. Scale bar, 5 μm.

(b) Schematic diagram of the experimental procedure for immunization with Spike-loaded eMigrasomes (eM-S) and collection of serum.

(c) Illustration of the rVSV-venus-SARS-CoV-2 system. VSV-Venus-SARS-CoV2 was mixed with vaccinated mice sera. Vero-TMPRSS2 cells were infected with the

505 reporter virus/serum mixture with an MOI of 0.01. 40 hrs post infection, the Venus-
506 positive infected cells were quantified to estimate the NT_{50} value for each serum.
507 (d) Spike-specific IgG was quantified in WT mice immunized with eM-S (20 μg/mouse,
508 *i.v.*) at different time points. Each symbol represents one individual animal.
509 (e) Neutralization curves are presented for sera from primary-vaccination and boost-
510 vaccination. Dots along the lines represent means from individual serum samples.
511 Nonlinear regression was performed using the equation for the normalized response
512 versus the inhibitor, incorporating a variable slope.
513 (f) NT_{50} of individual mouse in vaccinated groups were compared by p-value (Paired t-
514 test) are indicated. Dotted lines represent assay limits of detection. Each line represents
515 an individual mouse.
516

517 **Supplementary Information**

Figure S1

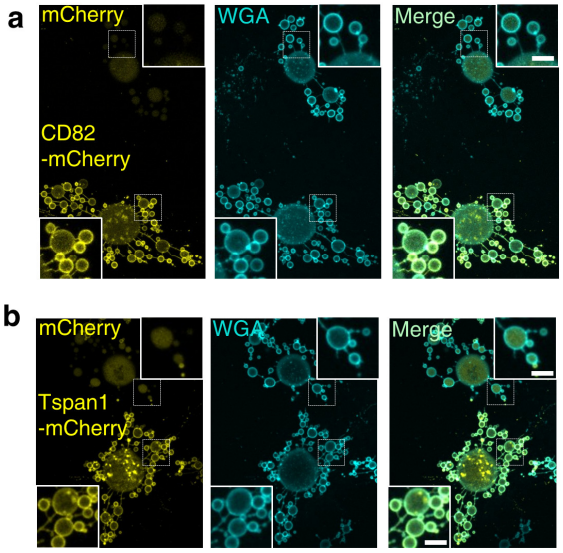

518 **Figure S1 | The effect of tetraspanin expression on the formation of migrasome-**

519 **like structures**

520 (a) NRK cells were transiently transfected with mCherry vector or CD82-mCherry. The

521 cells were then treated and imaged as described in Fig 2a.

522 (b) NRK cells were transiently transfected with mCherry vector or Tspan1-mCherry.

523 The cells were then treated and imaged as described in Fig 2a.

524

525 **Supplementary video legends**

526 **Supplementary video 1**

527 Time-lapse movie showing the biogenesis of migrasome-like structures. Related to

528 Figure 1a.

529 **Supplementary video 2**

530 The dynamic of migrasome-like structures induced by single-step approach. Related to

531 the upper panel of Figure 1e.

532 **Supplementary video 3**

533 The dynamic of migrasome-like structures induced by stepwise approach. Related to

534 the lower panel of Figure 1e.

535 **Supplementary video 4**

536 4D time-lapse movie showing the biogenesis of eMigrasomes.

537

538 **Materials and Methods**

539 **Molecular cloning**

540 The sequence spanning amino acids 252 to 289 of syntatin-2 (STX-2), which

541 incorporates the transmembrane domain along with the polybasic tail, was amplified

542 from mouse cDNA by polymerase chain reaction (NEB, M0492L) using primers below:

543 fwd:5'- atgaagaaagccatcaaataccagagc -3';

544 rev:5'- gcaccgatggagcccatcgagcctttgccaaccgacaagccaatg -3'.

545 The sequence of ovalbumin was amplified from the plasmid using primers below:

546 fwd: 5'- atgggctccatcggtgc -3';

547 rev: 5'- aggggaaacacatctgccaaag -3'.

548 Using $STX2_{252-289}$ and ovalbumin as templates, the membrane-tethered mOVA, in

549 which $STX2_{252-289}$ sequence is tagged to ovalbumin sequence, was further amplified

550 using the primers below:

551 fwd: 5'- tcagatctcgagctcaagcttatgaagaaagccatcaaataccagagc -3'

552 rev: 5'- tggtggcgaccggtggatcccggaggaagaacactaaggcagcaaaagagaag -3'

553 The fragment was inserted into pmCherry-N1 vector using a One Step Cloning Kit
554 (Vazyme, C112).

555 **Cell culture**

556 Cells were cultured at 37 °C with 5% CO_2. NRK cells and HEK 293FT cells were grown
557 in DMEM (Gibco, C11995500BT) supplemented with 10% (v/v) FBS (Biological
558 Industries), 1% (v/v) glutamax (Gibco, 35050-061) and 1% (v/v) penicillin–
559 streptomycin. MCA-205 cells were grown in RPMI 1640 (Gibco, C11875500BT)
560 supplemented with 10% (v/v) FBS, 1% (v/v) glutamax and 1% (v/v) penicillin–
561 streptomycin Vero-TMPRSS2 cells were maintained in DMEM supplemented with 10%
562 (v/v) FBS and 50 IU/ml penicillin-streptomycin. ADSC cells and BMSC cells were
563 grown in stem cell serum-free medium (CytoNiche, RMZ112).

564 **Cell transfection and cell line development**

565 For NRK cells, transfection was performed using electroporation (AMAXA,
566 Nucleofector). For MCA-205 cells, transfection was performed using Lipofectamine
567 3000 transfection reagent (Thermo Fisher Scientific, L3000015). In establish stable cell
568 lines, the transfected cells underwent initial selection with Hygromycin B (Roche,
569 10843555001) and were subsequently sorted into single colonies in 96-well plates via
570 flow cytometry.

571 **Imaging**

572 Confocal imaging of live cells and isolated eMigrasomes was performed using a Nikon
573 A1HD25 laser scanning confocal microscope. Cells were cultured in a confocal
574 chamber (Cellvis, D35-20-1-N or D35C4-20-1.5-N) that had been pre-treated with 10

575 μg/ml fibronectin (F0895) and allowed to proliferate overnight (14-18 hours). For
576 visualizing eMigrasomes, a small region in the confocal chamber was coated with a 10
577 μl drop of 10 μg/ml fibronectin. Following aspiration of the fibronectin, a 10 μl drop of
578 isolated eMigrasomes was dispensed into the coated area and left to settle for a
579 minimum of 1 hour prior to imaging. To prevent evaporation, the chamber was sealed
580 using parafilm.

581 **Real-time hypotonic stimulation**

582 To observe the dynamics of migrasome-like structures and eMigrasomes, a custom-
583 made buffer displacement device was utilized (refer to Fig 1d). Essentially, three
584 apertures were created on the lid of a confocal chamber to perfectly accommodate a
585 silicon microinjection tube with an external diameter of 1.9 mm. The silicon
586 microinjection tube was securely connected to a 1 ml syringe after the removal of its
587 sharp needle.

588 For a single-step stimulation process, two syringes were employed. One was kept empty,
589 while the other was filled with the desired hypotonic buffer. During time-lapse imaging,
590 the reservoir solution was aspirated using the empty syringe, and the hypotonic buffer
591 was simultaneously injected from the other syringe.

592 In the case of stepwise stimulation, three syringes were deployed. The first was loaded
593 with the initial buffer from the reservoir and was used to withdraw the reservoir solution.
594 The second syringe contained deionized water (ddH_2O) and was used to add a specific
595 volume of water at each step. The third syringe, which was empty, was used to ensure
596 thorough mixing of the reservoir solution after each stimulation event.

597 **Drug treatment**

598 For SMS2 inhibition, 30 min post seeding of the cells, the culture medium was gently
599 replaced with fresh medium containing either 25 μM SMS2-IN-1 (MCE, HY-102041)
600 or 0.25 (v/v) % DMSO. Cells were treated for 16 hrs prior to imaging.

601 For cholesterol extraction from *in situ* or isolated eMigrasomes, h-KDPBS containing
602 10 mM MβCD (Sigma, 332615) or 10 (v/v) % ddH_2O was applied. For *in situ*
603 eMigrasomes, z-stack images were collected after 30 min incubation at 37 °C. For
604 isolated eMigrasomes, buffer containing MβCD or ddH_2O was applied using the real-
605 time stimulation device described above. A 20-min time-lapse imaging session was
606 performed to capture the process of morphological changes in eMigrasomes.

607 **Permeability assay**

608 Isolated eMigrasomes were diluted in h-KPBS-BSA, containing 5 μg/ml of Cy5 and 25
609 μg/ml of 40kDa Dextran-TMR (D1842). A droplet of the eMigrasome solution was
610 prepared and imaged following the procedure described previously.

611 **Ion replacement assay**

612 The standard formulation of DPBS is 138 mM NaCl, 8.1 mM Na_2HPO_4, 2.7 mM KCl,
613 1.5 mM KH_2PO_4. In the ion replacement assay, as referenced in Figure S1d and S1e,
614 the 138 mM NaCl in DPBS was substituted with equal molar KCl, CsCl or Choline
615 chloride. The other three components were not changed.

616 The K-DPBS formulation utilized for eMigrasome production contains 140.6 mM KCl,
617 1.5 mM KH_2PO_4, 8.1 mM K_2HPO_4.

618 **Induction and purification eMigrasomes**

619 It's important to underscore that several critical parameters, such as the seeding density,
620 the working concentration of latrunculin A, and the incubation period, along with the
621 hypotonic gradient, should be individually optimized for each cell type. The quantities
622 of cells and reagents utilized should be modulated according to the flask size (examples
623 are provided in the following table).

Cell type	**NRK**	**MCA-205**	**ADCS**	**BMSC**
Seeding density (cells / cm^2)	1.5×10^4	3×10^4	2×10^4	2×10^4
Latrunculin A concentration (μM)	2	2	0.6	0.6
Latrunculin A incubation time (min)	10	45	20	20
Reduced osmolarity per step	1/6	1/4	1/6	1/6

624 In the following method, the purification of eMigrasomes from NRK cells cultured in
625 a single T75 flask (NEST, 708003) is used as a representative example. Three major
626 steps include cell preparation, eMigrasome induction and purification.

627 I. Cell Preparation

628 A T75 flask was coated with 4 μg/ml of fibronectin. 1×10^6 Cells were seeded into the
629 pre-coated flask, allowed to grow for 14-16 hours.

630 II. eMigrasome induction

631 Cortical actin disruption was achieved by discarding the culture medium and rinsing
632 the cells once with PBS. Then, 7.5 ml of K-DPBS containing 2 μM of Latrunculin-A
633 was added to the flask. The cells were incubated at 37°C in a 5% CO_2 atmosphere for
634 10 minutes.

635 Hypotonic stimulation was performed by placing the flask on an orbital shaker inside
636 the CO_2 incubator and adjusting the speed to 40 rpm. The stimulation was progressively

637 introduced by adding 1.5 ml, 1.8 ml, or 2.2 ml of deionized water at three-minute
638 intervals. Following this, the speed of the orbital shaker was increased to 60 rpm for
639 five minutes.

640 III. eMigrasome purification

641 First, the bubbles were harvested using the following procedure. The supernatant
642 containing cell bodies was discarded. The flask's bottom was gently washed once with
643 hK-DPBS (60% K-DPBS matching the current osmolarity). Subsequently, 4 ml of hK-
644 DPBS-BSA (60% K-DPBS containing 1 mg/ml BSA) was added to the flask. Gentle
645 pipetting was employed to detach the eMigrasomes, and the resultant solution was
646 collected into a conical tube. This step was repeated once, and the collected solutions
647 were combined.

648 To remove the remaining cell bodies, a process of differential centrifugation and
649 gravity-dependent filtration was used. Initially, the solution was centrifuged at 300 x g
650 at 4°C for 10 minutes, after which the supernatant was collected. The same process was
651 repeated at 500 x g for 10 minutes. The collected supernatant was poured into a filter
652 cup containing a pre-rinsed 6 μm parylene filter (Hangzhou Branemagic Medical
653 Technology, F-PAC007). The filter was pre-rinsed with 100% ethanol followed by hK-
654 DPBS-BSA. The flow-through was then collected in a low-protein-binding conical tube
655 (Eppendorf, 0030122240).

656 To concentrate the eMigrasomes, the solution was centrifuged at 20,000 x g at 4°C for
657 30 minutes. In the event of a large volume, a longer time may be necessary. The
658 supernatant was discarded, and the eMigrasome pellet was resuspended in PBS. The

659 protein concentration was determined using a BCA analysis, and the PBS volume was
660 adjusted to reach the desired eMigrasome concentration. For long-term storage, it was
661 recommended that the eMigrasomes were stored as a pellet, with a small volume of hK-
662 DPBS-BSA to cover it. This measure was adopted to minimize eMigrasome loss due
663 to container adsorption.

664 **Negative staining TEM**

665 Isolated eMigrasomes underwent fixation by the addition of an equal volume of 2.5%
666 glutaraldehyde (GA). A droplet of the fixed eMigrasome sample was deposited onto a
667 copper grid for 15 minutes. Excess sample was blotted off with filter paper. The grid
668 was promptly washed with a droplet of double distilled water (ddH_2O), stained with 1%
669 uranyl acid for one minute, and then further washed with two droplets of ddH_2O.
670 Remaining water was blotted off using filter paper and the grid was allowed to air-dry
671 fully before imaging was conducted via transmission electron microscopy (TEM).

672 **Cryo-EM sample preparation and image acquisition**

673 Quantifoil Cu grids (200 mesh, R2/2) underwent glow-discharging using a plasma
674 cleaning device (PDC-32G, Harrick Plasma). Each EM grid was applied with 4 μl
675 sample and vitrified by plugging into liquid ethane using the Vitrobot Mark IV system
676 (Thermo Fisher Scientific). The cryo-EM samples were examined using an FEI Tecnai
677 Arctica 200 kV transmission electron microscope, and images were captured at a
678 magnification of 23.5 kx using an FEI Falcon II direct electron detector, with a dose
679 approximately around 15 e−Å−2.

680 **eMigrasome quantification using flow cytometry**

681 Isolated eMigrasomes were suspended in h-KDPBS containing 1 μg/ml Wheat Germ
682 Agglutinin (WGA, Thermo, W11262). Various dilutions were prepared to ensure at
683 least one dilution had a concentration ranging from 1000 to 10000 eMigrasomes per μl.
684 Data were collected using a CytoFlex LX cytometer (Beckman). The threshold for
685 forward scatter (FSC) was manually set to 4000 to detect small particles. Events that
686 were double positive for B525-FITC and Y610-mcherry were gated as eMigrasomes.

687 **Size analysis by Hough Circle Transforming**

688 Size analysis of isolated eMigrasomes was conducted using ImageJ, complemented by
689 the Hough Circle Transform plugin. Sum slices processing of Z-stack was applied to
690 the 488 channel of the confocal images, representing the fluorescence signal from
691 Tspan4-GFP. The image was subsequently converted to an 8-bit grayscale. Edge
692 detection was performed using the "Find Edges" function to identify individual
693 eMigrasomes. Subsequently, the "Threshold" function was applied to encompass the
694 majority of the fluorescent signal from the eMigrasomes. Hough Circle Transform
695 analysis was then utilized with the following parameters: Easy mode; Minimum = 3
696 pixels; Maximum = 24 pixels; Hough score threshold = 0.9. All output options were
697 selected.

698 **Immunoblotting**

699 Cells or eMigrasomes were subjected to lysis using a 2% SDS solution in 50 mM Tris
700 buffer, followed by heating at 95 °C. The protein concentration of the samples was
701 assessed using a BCA kit (Vazyme, E112-02-AB). The lysates were diluted to the
702 desired concentration and then denatured via the addition of loading buffer (Beyotime,

703 P0015). The proteins were segregated by SDS-PAGE electrophoresis (Epizyme, PG112
704 or Yeasen, 36255ES10), and subsequently transferred to a 0.45 μm PVDF membrane
705 (Millipore, IPVH00010) in accordance with a standard protocol. The blot was blocked
706 with 5% milk in TBST and left to incubate overnight with the primary antibody at 4 °C.
707 The blot was then washed thrice with TBST and incubated with the secondary antibody
708 at room temperature for 1 hour. Finally, the blot underwent three more washes prior to
709 signal detection via chemiluminescence imaging (CYANAGEN, XLS070P or Thermo,
710 34075), utilizing a ChemiDoc MP Imaging System (Biorad).
711 Primary antibodies used for immunoblotting included: anti-integrin α5 (CST, 4705T),
712 anti-Na-K-ATPase (CST, 3010S), anti-histone H3 (CST, 4499S), anti-lamp2 (Sigma),
713 anti-calnexin (abcam, ab22595). anti-GFP (Roche, 11814460001 or abcam, ab290),
714 anti-GAPDH (Proteintech, 60004-1-Ig), anti-TIM23 (BD, 611222), anti-S1 (Sinobio,
715 40591-MM42), anti-ovalbumin (santa cruz, sc80587 or abcam, ab181688), anti-
716 mCherry (abcam, ab125096). Primary antibodies were diluted using Solution 1 (Takara,
717 NKB-101). Secondary antibodies used for immunoblotting included peroxidase
718 AffiniPure Goat Anti-Rabbit IgG (H+L) (Jackson ImmunoResearch, 111-035-003) and
719 peroxidase AffiniPure Goat Anti-Mouse IgG (H+L) (Jackson ImmunoResearch ,115-
720 035-003). Secondary antibodies were diluted using 5% milk in TBST.
721 **Mice**
722 WT C57BL/6 (Jax 000664) specific-pathogen-free (SPF) mice were procured from the
723 Laboratory Animal Center of Tsinghua University, China. The OT-II (Jax 004194)
724 mice were donated by Dr. Yan Shi. All the mice were bred and maintained under SPF

725 conditions at the Laboratory Animal Center of Tsinghua University, in accordance with
726 the National Institute of Health Guide for the Care and Use of Laboratory Animals.

727 **Immunization**

728 For systemic immunization, mice were intravenously administered eM-OVA dissolved
729 in 100 μL PBS, or intraperitoneally administered a mixture containing 50 μg OVA in
730 50 μL PBS (Sigma; A5503) and 50 μL Imject® Alum (Thermo; 77161). For nasal
731 immunization, mice were anesthetized using isoflurane and subsequently intranasally
732 administered 20 μg eM-OVA dissolved in 30 μL PBS. For subcutaneous immunization,
733 20 μg eM-OVA in 100 μL PBS was administered through injections on both sides of
734 the buttock.

735 **Enzyme linked immunosorbent assay (ELISA)**

736 Serum was prepared from whole blood by centrifugation. The levels of antigen-specific
737 antibody were determined using a direct ELISA method. Briefly, a 96-well plate were
738 coated overnight at 4 °C with antigen (2 μg/mL). The wells were then blocked with
739 PBS containing 10 % fetal calf serum before the addition of serially diluted serum.
740 Horseradish peroxidase-conjugated secondary antibodies were incubated for 1 hour at
741 room temperature. Between each step, wells were washed with PBST. The colorimetric
742 reaction was carried out using the 1-Step Ultra TMB-ELISA Substrate. The reaction
743 was stopped with 2 N H_2SO_4, and absorbance at 450 nm was read using a multimode
744 reader. For quantification of OVA-IgG and Spike-IgG, a standard curve was generated
745 using serially diluted anti-OVA antibody (Santa Cruz; sc-80589) and anti-Spike
746 antibody (Sino Biological; 40591-MM42), respectively.

747 **Fluorescence-based neutralization test**

748 Mouse sera were heat-inactivated at 56°C for a duration of 30 min. The indicated
749 dilutions of samples were mixed with $2x10^2$ FFU (Focus Forming Units) of VSV-
750 Venus-SARS-CoV-2 and incubated for 1 h at a temperature of 37°C. The mixture of
751 serum and virus were then added to Vero-TMPRSS2 cells grown on 96-well plates, and
752 incubated at 37°C for about 40 hours. The cells were then harvested and fixed in a 4%
753 paraformaldehyde solution for 20 min at room temperature. The fixed cells were
754 resuspended in PBS and analyzed using a LSRFortessa SORP (BD Biosciences) and
755 FlowJo software.

756 The Vero-TMPRSS2 cell line, which was constructed based on Vero (ATCC CCL-
757 81™), stably expressed the TMPRSS2 (Transmembrane Serine Protease 2) protein to
758 enhance the entry of the SARS-CoV-2 spike.

759 **Statistical analysis**

760 All data were subjected to analysis using GraphPad Prism statistical software. Unpaired
761 two-tailed t-tests or paired two-tailed t-tests were employed for the data analysis. The
762 results are represented as the mean ± standard error of the mean (s.e.m.). A *P* value of
763 less than 0.05 was deemed to indicate statistical significance.

764

765 **Competing interests**

766 L.Y. is the scientific founder of Migrasome Therapeutics.

767 L.Y., D.W., Takami.S., and Y.Z. are inventors on relevant patent applications held by
768 Migrasome Therapeutics. The remaining authors declare no competing financial
769 interests.
770

771 **Acknowledgements**

772 This research was supported by the National Key Research and Development Program
773 of China (2018YFE0207300), National Natural Science Foundation of China (grant no.
774 32030023), Beijing Municipal Science & Technology Commission, Administrative
775 Commission of Zhongguancun Science Park (grant no. Z221100003422012), Tsinghua
776 University Initiative Scientific Research Program (grant no. 20221080007). Sincere
777 gratitude is expressed towards Baidong Hou (Institute of Biophysics, Chinese Academy
778 of Sciences) for providing mouse strains and engaging in valuable discussions. We
779 thank the State Key Laboratory of Membrane Biology, SLSTU-Nikon Biological
780 Imaging Center, Laboratory of Animal Resources Center (THU-LARC), Tsinghua
781 University, for technical support. Acknowledgment is also given to the Research Fund
782 of the Vanke School of Public Health at Tsinghua University.
783

784 **Author contributions**

785 L.Y. and Z.L. supervised the project. The experiments were designed by L.Y., Z.L.,
786 Q.D., D.W., H.W., and Z.Z. D.W. carried out all the experiments related to the
787 discovery, development, and characterization of eMigrasomes. H.W. performed all the
788 animal experiments and immunological analyses. Z.Z. conducted pseudovirus

789 neutralization assays. W.W. participated in the immunological experiments. Takami. S.
790 and Y.Z. provided assistance with molecular biology and cell biology experiments. X.Z.
791 was responsible for collecting EM data. L.D. contributed to the purification of
792 eMigrasomes. The manuscript was written by L.Y. and Z.L., with input from all the
793 authors.
794

795 **References**

796 1. Park, J.W., Lagniton, P.N.P., Liu, Y. & Xu, R.H. mRNA vaccines for COVID-19: what, why
797 and how. *International journal of biological sciences* **17**, 1446-1460 (2021).
798 2. Polack, F.P. et al. Safety and Efficacy of the BNT162b2 mRNA Covid-19 Vaccine. *N Engl J*
799 *Med* **383**, 2603-2615 (2020).
800 3. Baden, L.R. et al. Efficacy and Safety of the mRNA-1273 SARS-CoV-2 Vaccine. *N Engl J*
801 *Med* **384**, 403-416 (2021).
802 4. Gui, Y. et al. Safety and immunogenicity of a modified COVID-19 mRNA vaccine,
803 SYS6006, as a fourth-dose booster following three doses of inactivated vaccines in
804 healthy adults: an open-labeled Phase 1 trial. *Life Metabolism* **2**, load019 (2023).
805 5. Crommelin, D.J.A., Anchordoquy, T.J., Volkin, D.B., Jiskoot, W. & Mastrobattista, E.
806 Addressing the Cold Reality of mRNA Vaccine Stability. *Journal of pharmaceutical*
807 *sciences* **110**, 997-1001 (2021).
808 6. Grau, S., Ferrández, O., Martín-García, E. & Maldonado, R. Reconstituted mRNA COVID-
809 19 vaccines may maintain stability after continuous movement. *Clinical microbiology*
810 *and infection : the official publication of the European Society of Clinical Microbiology*
811 *and Infectious Diseases* **27**, 1698.e1691-1698.e1694 (2021).
812 7. Ma, L. et al. Discovery of the migrasome, an organelle mediating release of cytoplasmic
813 contents during cell migration. *Cell Res* **25**, 24-38 (2015).
814 8. Wu, D. et al. Pairing of integrins with ECM proteins determines migrasome formation.
815 *Cell Res* **27**, 1397-1400 (2017).
816 9. Huang, Y. et al. Migrasome formation is mediated by assembly of micron-scale
817 tetraspanin macrodomains. *Nat Cell Biol* **21**, 991-1002 (2019).
818 10. Ding, T. et al. The phosphatidylinositol (4,5)-bisphosphate-Rab35 axis regulates
819 migrasome formation. *Cell Res* (2023).
820 11. Dharan, R. et al. Tetraspanin 4 stabilizes membrane swellings and facilitates their
821 maturation into migrasomes. *Nat Commun* **14**, 1037 (2023).
822 12. Huang, Y., Zhang, X., Wang, H.W. & Yu, L. Assembly of Tetraspanin-enriched
823 macrodomains contains membrane damage to facilitate repair. *Nat Cell Biol* **24**, 825-
824 832 (2022).
825 13. Levy, S. & Shoham, T. The tetraspanin web modulates immune-signalling complexes.

Nat Rev Immunol **5**, 136-148 (2005).
14. CHARRIN, S. et al. EWI-2 is a new component of the tetraspanin web in hepatocytes and lymphoid cells. *Biochemical Journal* **373**, 409-421 (2003).
15. Clark, K.L., Zeng, Z.-M., Langford, A.L., Bowen, S.M. & Todd, S.C. PGRL Is a Major CD81-Associated Protein on Lymphocytes and Distinguishes a New Family of Cell Surface Proteins1. *The Journal of Immunology* **167**, 5115 - 5121 (2001).
16. Lefranc, M.-P. & Lefranc, G. The Immunoglobulin FactsBook. (2001).
17. Zucker, B. et al. Migrasome formation is initiated preferentially in tubular junctions by alternations of membrane tension or intracellular pressure. *bioRxiv*, 2023.2008.2003.551756 (2023).
18. Yoshikawa, K., Saito, S., Kadonosono, T., Tanaka, M. & Okochi, M. Osmotic stress induces the formation of migrasome-like vesicles. *FEBS Letters* (2024).
19. Hoffmann, E.K., Lambert, I.H. & Pedersen, S.F. Physiology of cell volume regulation in vertebrates. *Physiol Rev* **89**, 193-277 (2009).
20. Qiu, Z. et al. SWELL1, a plasma membrane protein, is an essential component of volume-regulated anion channel. *Cell* **157**, 447-458 (2014).
21. Voss, F.K. et al. Identification of LRRC8 Heteromers as an Essential Component of the Volume-Regulated Anion Channel VRAC. *Science* **344**, 634-638 (2014).
22. Chen, L., Ma, L. & Yu, L. WGA is a probe for migrasomes. *Cell Discov* **5**, 13 (2019).
23. Case, J.B. et al. Neutralizing Antibody and Soluble ACE2 Inhibition of a Replication-Competent VSV-SARS-CoV-2 and a Clinical Isolate of SARS-CoV-2. *Cell Host & Microbe* **28**, 475-485.e475 (2020).
24. Case, J.B. et al. Replication-Competent Vesicular Stomatitis Virus Vaccine Vector Protects against SARS-CoV-2-Mediated Pathogenesis in Mice. *Cell Host Microbe* **28**, 465-474 e464 (2020).
25. Jiang, D. et al. Migrasomes provide regional cues for organ morphogenesis during zebrafish gastrulation. *Nat Cell Biol* **21**, 966-977 (2019).
26. Zhang, C. et al. Monocytes deposit migrasomes to promote embryonic angiogenesis. *Nat Cell Biol* **24**, 1726-1738 (2022).
27. Zhu, M. et al. Lateral transfer of mRNA and protein by migrasomes modifies the recipient cells. *Cell Res* **31**, 237-240 (2021).
28. Jiao, H. et al. Mitocytosis, a migrasome-mediated mitochondrial quality-control process. *Cell* **184**, 2896-2910 e2813 (2021).